UDK 620.1:621.78.019.84:691.714.018.8
Original scientific article/Izvirni znanstveni članek

ISSN 1580-2949
MTAEC9, 55(2)317(2021)

FLUID-INDUCED ELECTROCHEMICAL CORROSION OF 13Cr STAINLESS STEEL IN HIGH-SPEED FLOWING LIQUID CONTAINING 1 *w*/% AND 2 *w*/% NaCl

KAPLJEVINSKO INDUCIRANA ELEKTROKEMIJSKA KOROZIJA NERJAVNEGA JEKLA S 13 % Cr V HITRO PRETAKAJOČI SE KAPLJEVINI Z VSEBNOSTJO 1 *w*/% IN 2 *w*/% NaCl

Hailong Jiang[1], Kui Zhang[2*], Boyu Jiang[3], Xuejin Dai[4]

[1]School of Mechanical Engineering, Xi'an Shiyou University, Xi'an City 710065, China
[2]CNPC Engineering Technology R&D Company Limited, Beijing City 102206, China
[3]Xi'an Branch of China Petroleum Materials Co. LTD, Xi'an City 710016, China
[4]No.5 Oil Production Plant, CNPC Qinghai Oilfield Company, Mangya City 816400, China

Prejem rokopisa – received: 2020-10-28; sprejem za objavo – accepted for publication: 2020-12-29

doi:10.17222/mit.2020.209

In order to study the electrochemical corrosion law for the 13Cr stainless-steel tubing material in a high-speed Cl-containing liquid, a high-speed-flow experiment and a small three-electrode system, embedded in a small pipe, were used. The open circuit potential (OCP), polarization curve (PC) and electrochemical impedance spectroscopy (EIS) of the stainless-steel surface were tested in a medium with a flow velocity ranging from 10 to 22 m/s containing 1 *w*/% and 2 *w*/% of NaCl. By comparing it with the changes in the electrochemical-reaction parameters of the material in distilled water, the results of the experiment including the critical flow velocity, the change of corrosion rate and the electrochemical-reaction control steps were obtained. By theoretically solving the frictional force of the liquid against the wall surface and the adsorption capacity of the oxide film, and assuming that the oxide film is a macromolecular combination, the relationship between the adsorption capacity of different surface films and the critical flow velocity in the high-speed pipe flow was established. The results of this experiment and calculation can provide a preliminary prediction of the critical flow velocity corresponding to the inflection point of the wall-surface corrosion rate in an industrial pipe flow, thereby improving the process parameters and reducing the wall damage.

Keywords: flow-induced corrosion, full-scale flow experiment, critical flow velocity, adsorption capacity of an oxide film

Avtorji so, zato da bi lahko študirali zakone elektrokemijske korozije v ceveh iz nerjavnega jekla vrste 13Cr pri velikih hitrostih pretoka kapljevine (vodne raztopine), ki vsebuje Cl, izvedli nadzorovane preizkuse pretoka z majhnim tri-elektrodnim sistemom, obdajajoč majhno cevčico. V zelo hitrem pretoku (med 10 m/s in 22 m/s) vodne raztopine, ki je vsebovala 1 *w*/% oziroma 2 *w*/% NaCl, so določali potencial odprtega kroga (OCP) in polarizacijsko krivuljo (PC) ter izvajali elektrokemijsko impedančno spektroskopijo (EIS) površine nerjavnega jekla. S primerjavo rezultatov eksperimenta in elektrokemijskih reakcijskih parametrov materiala ter destilirane vode, so lahko ugotovili spremembe korozijske hitrosti in kontrolne faze elektrokemijskih reakcij. S teoretično rešitvijo sile trenja kapljevine na površini stene cevčice in adsorpcijsko kapaciteto oksidnega filma s predpostavko, da je le-ta makro-molekularna kombinacija, so določili zvezo med adsorpcijsko kapaciteto različnih tankih površinskih plasti (filmov) in kritično hitrostjo pretoka v eksperimentalni cevčici po kateri se je pretakala Cl raztopina z veliko hitrostjo. Rezultati predstavljenih preizkusov in izračunov so avtorjem omogočili preliminarno napoved kritične hitrosti pretoka pri kateri nastopi točka preloma v hitrosti korozije površine. To omogoča izboljšanje procesnih parametrov in zmanjšanje števila poškodb na stenah industrijskih cevi.

Ključne besede: pretok kapljevine, inducirana korozija, nadzorovan preizkus pretoka, kritična hitrost pretoka, adsorpcijska kapaciteta oksidnega filma

1 INTRODUCTION

Flow-induced corrosion (FIC), or flow-accelerated corrosion (FAC), means that the fluid affects the corrosion reaction by changing the wall shear force or the mass transfer rate of the reactant.[1,2] On the one hand, the physical cutting of a wall by a fluid changes the structure of the corrosion-product film, on the other hand, it also changes the convection and diffusion rate of the reactants near the wall.[3] This phenomenon occurs frequently in an actual production and it is difficult to analyze because its research involves factors such as fluid flow, mass transfer, and electrochemical reactions. Especially for an environment with a high flow velocity and multiple media, the instability of the flow and the reversibility of the electrochemical reaction make it difficult to carry out measurements and calculations.

For the materials dominated by activation reactions, convection and diffusion of reactants are the main factors affecting the electrochemical reaction rate. A. Neville[4] described the liquid disturbance process near the wall as a continuous action, which includes the stages of extension, speed difference generating a vortex and liquid cutting of the wall. In this study, the laser Doppler test was used to observe the flow of liquid in the viscous bottom layer and the generation of vortex. S. Nesic[5] used an

*Corresponding author's e-mail:
cjr88112@163.com (Kui Zhang)

electrochemical-corrosion test in a flowing liquid to test the corrosion law on carbon steel in a medium containing CO_2. The results of this study explained:

1) when an increased rate of mass transfer of corrosive species, such as H^+ ions, to the steel surface leads to an acceleration of the cathodic reactions and a higher corrosion rate and

2) when an increased rate of mass transfer of the corrosion product, ferrous ions (Fe^{2+}), away from the steel surface makes it harder to form protective ferrous carbonate layers. If the concentration of the reactants determines the progress of the electrochemical reaction system, the fluid-flow factors are not negligible in the study.

X. Y. Yong et al. and J. J. Liu et al.[6,7] used carbon steel as the tested sample to measure the coefficient of action in static and changing flow-rate environments. The electrode reaction coefficient was measured in a nitrogen-charged and oxygen-depleted environment. The results showed that an increase in the flow rate increased the reaction rate of the carbon steel cathode.

For the materials dominated by passivation reactions, the oxide film on the surface can prevent some large molecules from passing through and inhibiting the cathode reaction. However, in the cases of external factors, such as the fluid shear force or physical impact, the product film rupture and regeneration process will occur on the material surface. F. Mohammadi and J. Luo[8] and Lu conducted a number of studies on the changes of the electrochemical reaction on the surface of stainless steel during a particle impact including the effect of velocity,[8] effect of particle-impact angle[9] on the electrochemical reaction and surface repassivation after the particle impact.[10] The theoretical solution and step test are used in these studies, and the time function of the current density and electric potential is obtained. Due to the fluid-flow state, local-pipe structure changes and the influence of the electrochemical reaction process, a parameter step also appears in the stainless-steel wall surface during a steady flow.[11] Z. B. Zheng et al.[12] carried out experiments to study the transient change of passivation and critical flow velocity (CFV). The results showed that the CFV was affected by the liquid flow rate, particle concentration and material properties. At the same time, the study proves that stainless steel has good corrosion resistance at most flow velocities. However, once a liquid contains a high concentration of Cl-, the protective effect of the product film is reduced because of the strong Cl^- penetration.[13]

13Cr stainless steel (or 13Cr-110) is a commonly used material for downhole tubing in an oil field in order to reduce corrosion failure. It can be used in a weak acid or a medium containing a small amount of Cl^- for a long-term service. However, for high-concentration Cl-medium high-speed flow conditions, a high wall shear stress and a heavy concentration of Cl^- cause severe corrosion and pitting corrosion of a 13Cr pipe wall.[14] In this paper, an integrated three-electrode system was used to measure the wall electrochemical parameters in a high-speed liquid flow. The short distance between the reference electrode and the working electrode as well as the larger auxiliary electrode area ensured the stability in the test process. In addition, the reason for the critical flow velocity and its variation rule was analyzed theoretically.

2 EXPERIMENTAL PART

2.1 Experimental set-up

As shown in Figure 1, the experimental loop comprised a perforating test section, screw pump (a flow range of 1–14 m^3/h), electric heating agitator, temperature and pressure sensor, magnetic flowmeter (8712HR, Rosemount Co., USA), three gate valves, control cabinet, computer and two flow pipes. After the perforating fluid containing sand was mixed well, stirring and electric heating were turned on until the desired temperature was reached. Then, the pump was opened. The three gate valves of the test pipe were opened when the flow became stable, and data such as particle-motion image, flow pressure and temperature were recorded.

To facilitate photographic documentation, an organic glass was used as the test device (**Figure 2**). A three-electrode system was incorporated into the flange for the open-circuit potential and potentiostatic testing. As

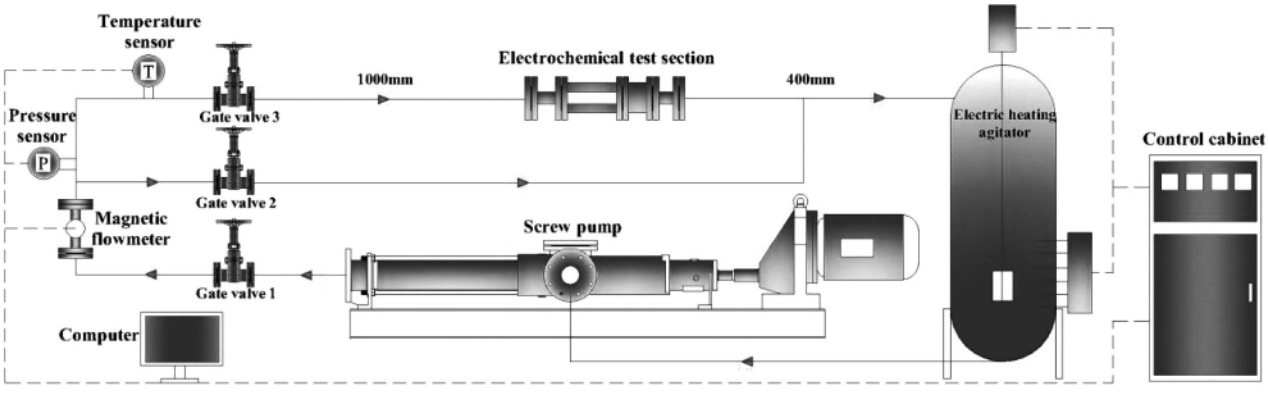

Figure 1: Electrochemical experimental loop

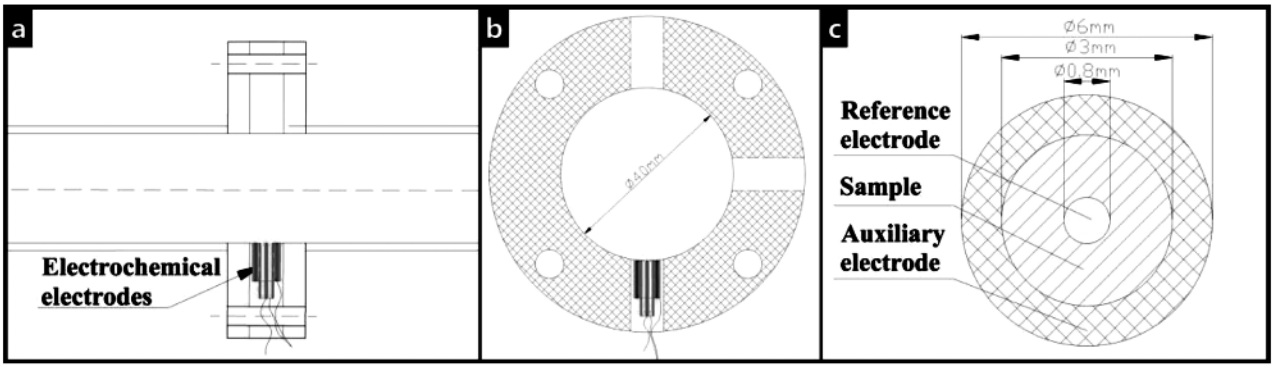

Figure 2: Schematic of the three-electrode system: a) axial schematic of the electrode-installation location; b) radial schematic of the electrode-installation position; c) three-electrode arrangement

shown in **Figure 2c**, the saturated calomel reference electrode (SCE), placed in the sample, was connected to a standard three-electrode system. The sample had been cut from a 3.5-inch (88.9 mm) 13Cr tubing with a diameter of 3 mm and a thickness of 10 mm. Ring-shaped graphite was used as the auxiliary electrode (AE). Before doing the experiment, the exposed surface was sealed with epoxy resin and ground using SiC emery paper of grade 1200 prior to installation. A multi-channel electrochemical workstation (PARSTAT MC, USA) was used for electrochemical testing. A JSM-6390 stereo microscope (JEOL, Japan) with a frame rate of 50 fr/s was used to document micro-erosion maps of the sample surface.

2.2 Materials

The composition and mechanical properties of the 13Cr stainless are shown in **Tables 1** and **2**, respectively. Electrolyte solutions of 1 *w*/% and 2 *w*/% of sodium chloride (NaCl) in double distilled water were used as the circulation media. The velocities of the particles changed from 10 m/s to 22 m/s. Seven flow velocities were designed for the comparison between the 1*w*/% NaCl solution and 2 *w*/% NaCl solution.

Table 1: Chemical composition of 13Cr stainless steel (*w*/%)

Material	C	Si	Mn	P	S	Cr	Mo	Ni	Cu
13Cr	0.029	0.22	0.45	0.015	0.001	13.3	1.92	4.85	1.59

Table 2: Mechanical properties of 13Cr stainless steel

Material	Tensile strength (MPa)	Yield strength (MPa)	Elongation (%)	Hardness (HV)
13Cr	970	855	20	323.4

3 RESULTS

3.1 Open circuit potential and current density

The open circuit potential method (OCP) is used to measure the potential difference between the corrosion micro-potential and the reference electrode in an environment of stable and natural conditions without an applied current. **Figures 3** and **4** show the results of measuring the open circuit potential and corresponding current density of the 13Cr surface in the flowing liquid. In different media, the OCP of the 13Cr steel surface decreases with the increasing flow velocity. The comparison results of the potential test of distilled water and Cl-containing water show that the potential increases positively after adding Cl^- and there is a step potential that changes with the flow velocity. The step potential in distilled water corresponds to a flow velocity close to 16 m/s, while in Cl-containing liquids, it is 18 m/s. Meanwhile, the potential steps in distilled water, the liquid containing 1 *w*/% NaCl and 2 *w*/% NaCl are 0.1 V, 0.09 V and 0.14 V, respectively, which indicates that the increase in the Cl-concentration increased the potential step of the local flow rate.

Comparing the thermodynamic characteristics of the OCP in a high-speed flowing liquid, the current density of the circulating circuit in the material is shown in **Figure 4**. The difference between the current change and potential change is the fact that the current density corresponding to each flow rate is close to the other one from distilled water, while the current density of the Cl-containing liquid has a significant step process. The current-density step values for the liquids containing 1 *w*/% NaCl and 2 *w*/% NaCl are 0.025 and 0.026 mA, which shows that the addition of Cl^- causes a local step, while the current under high-concentration conditions tends to stabilize.

By applying the polarization potential, the polarization curve obtained by scanning the moving point is shown in **Figure 5**. When distilled water does not contain Cl^-, the E-log**I** anode curve corresponding to each flow velocity has no obvious passivation area, which indicates that the 13Cr surface cannot be completely passivated at the high-speed flow and the reaction is in a dynamic equilibrium state. Through Tafel fitting, the change law for the corrosion rate with the flow velocity shown in **Figure 5b** is obtained. The results show that the corrosion rate of 13Cr in the Cl-free flowing liquid is

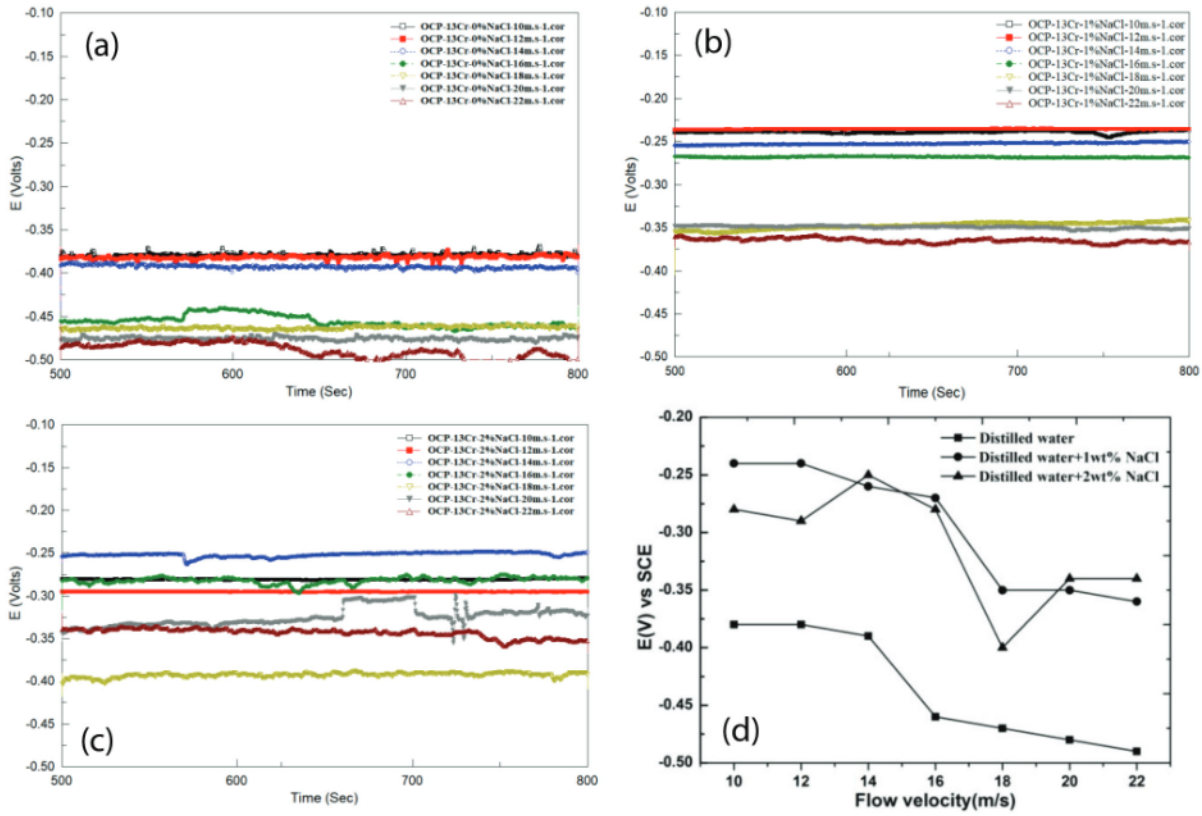

Figure 3: Surface potential diagram of 13Cr under different media and flow velocities: a) distilled water, b) distilled water +1 *w*/% NaCl, c) distilled water +2 *w*/% NaCl, d) potential comparison chart

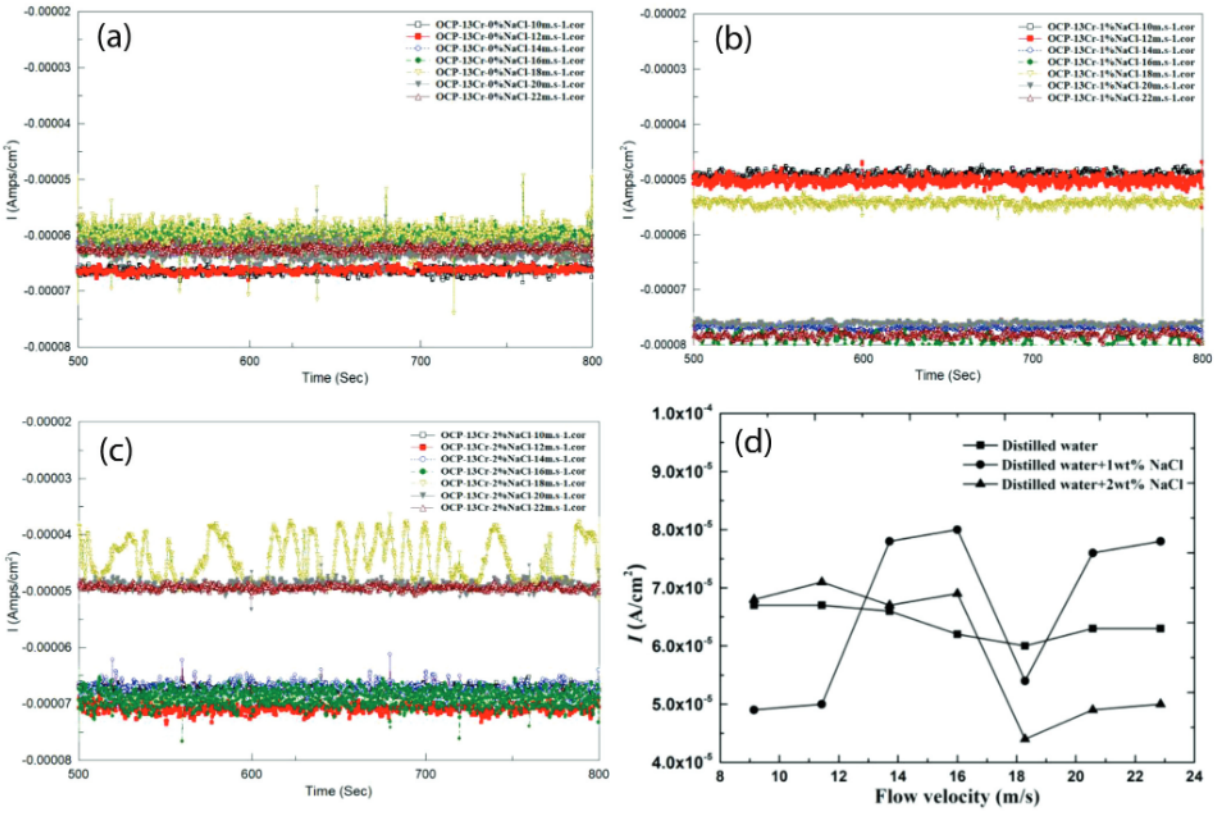

Figure 4: Surface-current-density diagram of 13Cr under different media and flow velocities: a) distilled water, b) distilled water + 1 *w*/% NaCl, c) distilled water + 2 *w*/% NaCl, d) potential comparison chart

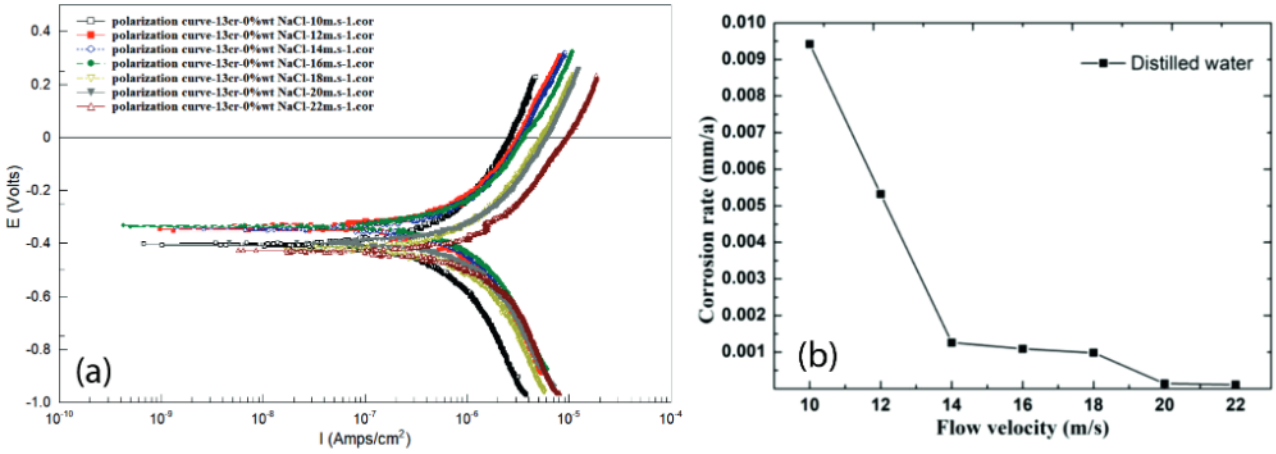

Figure 5: Surface-polarization curve of 13Cr in distilled water: a) polarization curves b) corrosion rate

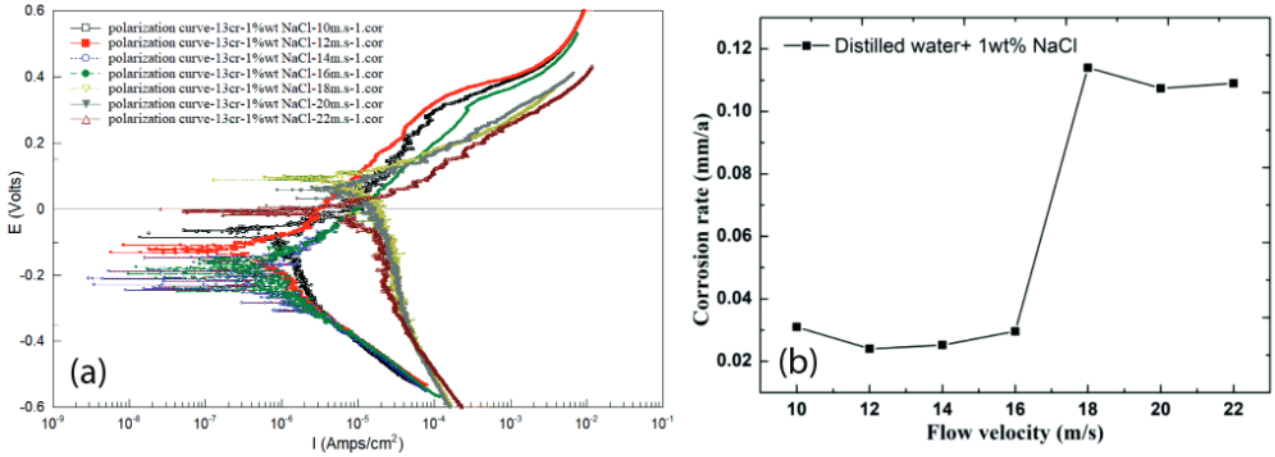

Figure 6: Surface-polarization curves of 13Cr in distilled water containing 1 *w*/% NaCl: a) polarization curves, b) corrosion rate

less than 0.1 mm and the corrosion rate tends to be stable at a flow velocity greater than 14 m/s. Therefore, the corrosion rate of the 13Cr steel in flowing distilled water decreases as the flow rate increases, and eventually stabilizes in a minimum value interval.

As shown in **Figures 6** and **7**, when NaCl was added to the distilled water, the corrosion rate, the slope of the cathode and anode polarization curves changed significantly. When the flow velocity is less than 16 m/s, the corrosion rate of 13Cr in 2 *w*/% NaCl is almost three times that in 2 *w*/% NaCl, and when the flow velocity is greater than 18 m/s, the corrosion rates under the two Cl^- concentrations are similar. This shows that when the flow velocity is lower than the critical flow velocity, the

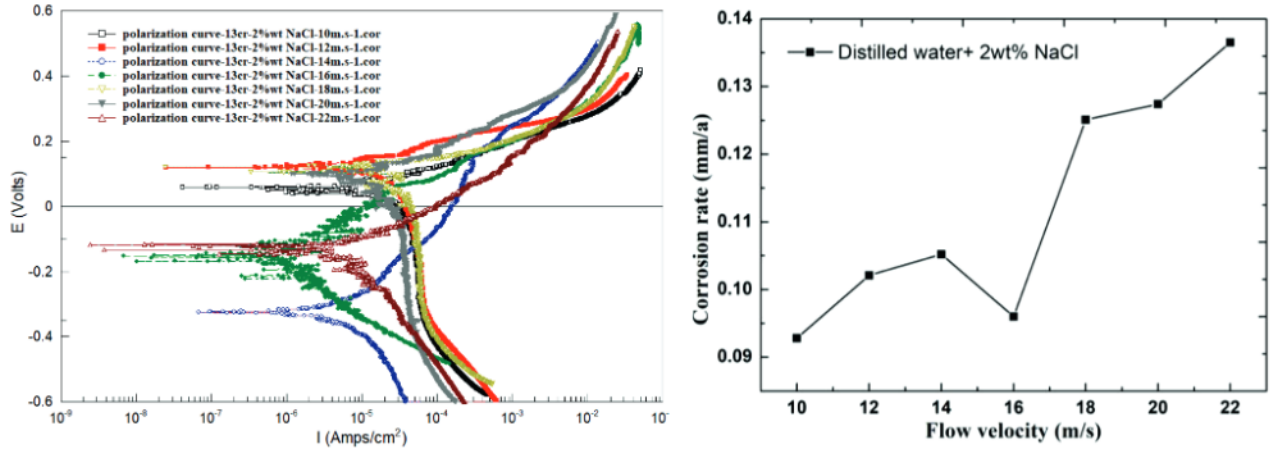

Figure 7: Surface-polarization curve of 13Cr in distilled water containing 2 *w*/% NaCl: a) polarization curves, b) corrosion rate

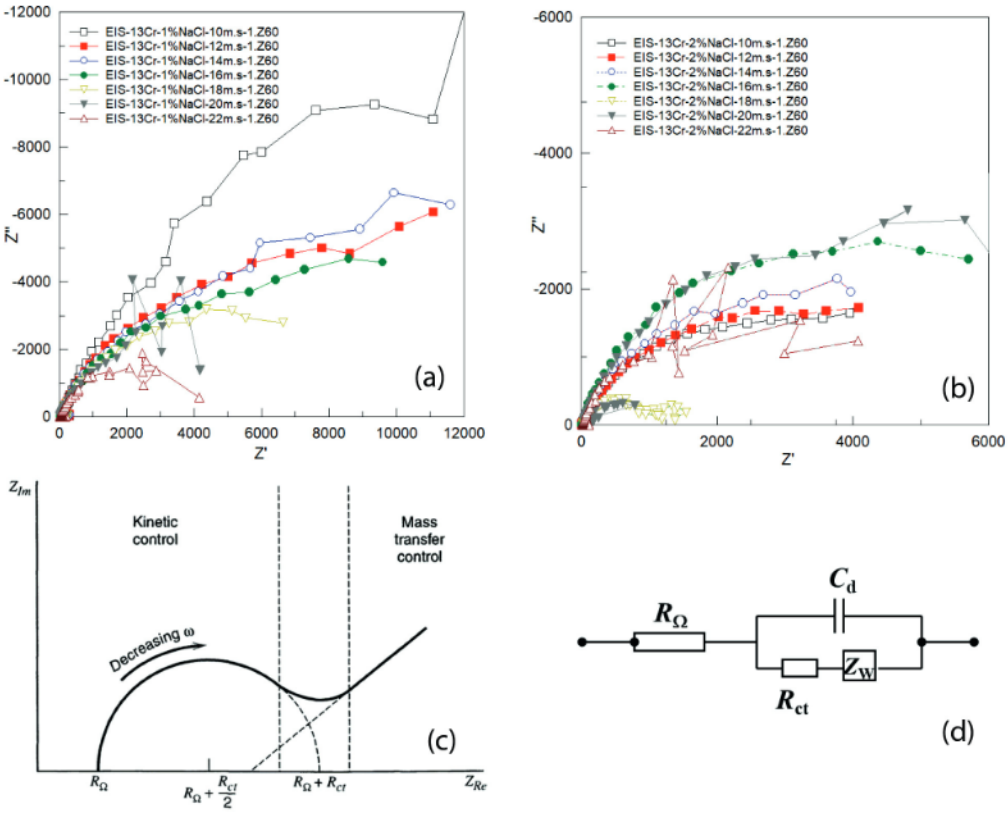

Figure 8: Nyquist plots for 13Cr stainless steel in a flowing liquid containing NaCl where R_Ω is solution resistance, R_{ct} is charge-transfer resistance, Z_w is diffusion resistance and C_d is a double-layer capacitor: a) distilled water +1 *w*/% NaCl, b) distilled water + 2 *w*/% NaCl, c) diagram of the Nyquist plot, d) equivalent circuit

presence of Cl^- has a great effect on the corrosion of 13Cr in the flowing liquid, and when it is greater than this flow velocity, the effect is weakened. In addition, when distilled water contains Cl^-, the absolute values of the slopes of the polarization curves at different flow velocities decrease. The increase in the current density corresponding to the same potential scan interval indicates that the anode dissolution reaction is accelerated. The slope of the 13Cr-cathode curve in a low-flow-rate (<16m/s) environment decreased significantly, which shows that the cathode reaction changed from the concentration control of the reactants to the mixing or electrochemical polarization control. At high flow velocities (>18m/s), the cathode reaction is mainly controlled by the mass transfer of the reactants.

By measuring Nyquist plots on the surface of 13Cr under the interference of sinusoidal potential, the changes in immittance at different flow velocities, as shown in **Figures 8a** and **8b**, are obtained. The results show that at most flow velocities, a 13Cr surface is controlled by electrochemical-reaction electron migration and reactant diffusion. A Nyquist plot is composed of a semicircle in the high-frequency region and a straight line with a slope of 45 degrees in the low-frequency region (**Figure 8c**). When Z'<4000 in the 1 *w*/% NaCl solution, the reaction is mainly controlled by the charge transfer, while the corresponding 2 *w*/% NaCl solution is Z'<2000. This indicates that when the Cl-concentration increases, the influence of reactant-diffusion factors increases. At the same time, according to the difference in the slope of the diffusion-affected-zone curve in the Nyquist figure, it can be found that the increase in the flow velocity and Cl-concentration causes the slope to decrease. Since this slope is affected by the convex radius of the material surface, a smaller radius indicates that the local reactant diffusion is equivalent to spherical diffusion in an environment of a high flow velocity and high Cl-concentration.

4 DISCUSSION

From the above test results, it is found that:

1) when a high concentration of Cl^- is added to distilled water, steps of electric potential, current density and corrosion rate appear on the surface of the 13Cr steel. At the same time, the critical flow rate corresponding to the step amount is less affected by the Cl^- concentration.

2) When Cl^- is added to distilled water, the cathode reaction changes from diffusion control of the reactant to mixing control, and the control factors of the reaction at different flow rates change significantly.

3) The change law for the corrosion rate of 13Cr in distilled water and the one for the Cl-containing liquid are opposite to each other. In the high-speed Cl-containing liquid, complex dissolution and passivation reactions occur on the surface of the material. The presence of Cl^- not only accelerates the local film dissolution, but also local enrichment and weakening of the reaction. Therefore, the structural change of the stainless-steel surface layer in a high-speed liquid environment is a process, in which physical properties change and electrochemical reactions act together.

By comparing the adsorption force and the liquid shear force of the stainless-steel film, the critical flow rate for the film dissolution can be obtained. According to the classical fluid-mechanics theory, the calculation of the shear force on the pipe wall in a laminar liquid and turbulent liquid can be expressed with Equations (1) and (2):

laminar flow

$$F_f\ S\tau_w \Delta L = \frac{4S\pi\mu u^a \Delta L}{r_i} \tag{1}$$

turbulent flow

$$F_f = S\tau_w \Delta L = 0.03 S\rho_c \Delta L (u^a)^{7/4} \left(\frac{\mu}{\rho_c r_i}\right)^{1/4} \tag{2}$$

When the metal surface is covered with the oxidation product film, the reactant needs to pass through the film and enter the lower layer to contact the metal to react. At this time, as the reaction proceeds, new oxides continue to be deposited to thicken the film. If distance y from the vertical wall represents the film thickness, the film growth rate is dy/dt. According to the definition of the mass-transfer flux:

$$J = -D\frac{\mathrm{d}C}{\mathrm{d}x} = -C\frac{\mathrm{d}x}{\mathrm{d}t} \tag{3}$$

and the film growth rate can be expressed as:

$$\frac{\mathrm{d}y}{\mathrm{d}t} = \frac{D\Delta C}{C_0 y} \tag{4}$$

where $\Delta C = C_W - C_O$ is the difference in the oxide concentration in the film. Integrate the two sides of the above formula to get the following result:

$$y = \sqrt{\frac{2D\Delta C t}{C_0}} \tag{5}$$

As the dense part of the oxide film is thin (nanolevel), the concentration difference ΔC is close to C_O, so the ratio between the two is close to 1. Therefore, the film thickness Equation (5) can be simplified as:

$$y = \sqrt{2D_{film} t} \tag{6}$$

where D_{film} is the oxide-diffusion coefficient for the thin layer. According to the Arrhenius equation,[15] the relationship between the diffusivity and the film charge number is obtained with the following formula:

$$D_{film} = D\exp\left(-\frac{Q_e}{RT}\right) \tag{7}$$

Film growth is a dynamic process that changes with the growth of the film potential and current density. Therefore, according to the Cottrell equation[16] of the potential step process, the relationship between the change in the electric quantity of the film and time is expressed by:

$$Q_e = \frac{2nFA_e D_{film}^{1/2} C_0 t^{1/2}}{\pi^{1/2}} \tag{8}$$

Substitute Equations (8) and (7) into Equation (6) to get the expression of the film thickness growth rate as shown below:

$$y = \sqrt{2tD\exp\left(\frac{2nFA_e D_{film}^{1/2} C_0 t^{1/2}}{RT\pi^{1/2}}\right)} \tag{9}$$

The film-surface adsorption force mainly includes the van der Waals force, electrostatic force and chemical affinity, in which the physical adsorption energy reaches 0.5 cv, about 10^{-3}~10^{1} N·cm^{-2}. According to the common expression of the Lennard-Jones potential energy,[17] $E_e = -\Lambda/z^6$, where Λ is a constant and z is the molecular distance, the total potential energy of the van der Waals force between the two particles is:

$$E_e = \frac{n_e^2\pi^2\Lambda}{6}\left[\frac{2r_1 r_2}{R_e^2-(r_1+r_2)^2} + \frac{2r_1 r_2}{R_e^2-(r_1-r_2)^2} + \ln\frac{R_e^2-(r_1+r_2)^2}{R_e^2-(r_1-r_2)^2}\right] \tag{10}$$

Where $H_e = n^2p^2\Lambda$ is the Hamaker constant[18], generally between 10^{-20}–10^{-19} J. When solving the van der Waals force between the particle and the wall, we have to set one of the particle radius to infinite, which means $r_2 \to \infty$; then the van der Waals potential energy of the particle and the wall is:

$$E_e = -\frac{H_e}{6}\left[\frac{d_p}{2y} + \frac{d_p}{2(yd_p)}\right] \tag{11}$$

When the film thickness is much larger than the particle diameter, the van der Waals potential energy becomes $E_e = -H_e d_p / 12y$. Therefore, the van der Waals force of surface film molecules or locally adsorbed particles is:

$$F_v = -\frac{H_e d_p}{12z^2} \tag{12}$$

The number of molecules per unit volume of the film can be expressed as:

$$N_e = n_e N_A = \frac{m_{x0} N_A}{M_{x0}} \tag{13}$$

In commonly used stainless-steel materials, the surface dense layer is generally composed of NiO and Cr_2O_3. Substitute the number of matter molecules into

Equation (5) to obtain the van der Waals force of the film adhesion as shown below:

$$F_{\mathrm{v}} = -\frac{H_{\mathrm{e}} d_{\mathrm{p}}}{12z^2} \cdot \frac{\rho_{x0} V_{x0} N_{\mathrm{A}}}{2A_{\mathrm{e}}^2 y^2 \varepsilon_{\mathrm{e}}} \tag{14}$$

The electrostatic adsorption force of the film can be expressed as:

$$F_{\mathrm{e}} = \frac{\sigma_{\mathrm{e}}^2}{2\varepsilon} = \frac{Q_{\mathrm{e}}^2}{2A_{\mathrm{e}}^2 y^2 \varepsilon_{\mathrm{e}}} \tag{15}$$

Therefore, the functional relationship of the film adhesion per square millimeter with the reaction time is:

$$F_{\mathrm{q}} = F_{\mathrm{v}} + F_{\mathrm{e}} = \frac{A_{\mathrm{e}} d_{\mathrm{p}}}{24y^2} \cdot \frac{Q_{\mathrm{e}}^2}{2A_{\mathrm{e}}^2 y^2 \varepsilon_{\mathrm{e}}} \tag{16}$$

Based on the film adsorption force for different film thicknesses, the critical flow velocity required for the films of different thicknesses to rupture is calculated and showed in Figure 9 where the relative molecular masses are $M_{Fe2O3} = 160$, $M_{NiO} = 74.6$, $M_{Cr2O3} = 152$ and the density values are $\rho_{Fe2O3} = 5.24 \times 10^3$ kg·m^{-3}, $\rho_{Cr2O3} = 5.21 \times 10^3$ kg·m^{-3}, $\rho_{NiO} = 6.67 \times 10^3$ kg·m^{-3}. Taking a 40-mm pipe diameter as the research object, the critical flow velocities of the film peeling corresponding to Fe_2O_3, Cr_2O_3 and NiO are shown in **Figures 9a** to **9 c**. Among them, due to the adsorption force where NiO > Cr_2O_3 > Fe_2O_3, the rupture critical flow velocity of the film with a large adsorption force is greater. The corresponding critical flow velocities of Fe_2O_3, Cr_2O_3 and NiO at a film thickness of 75.8 μm are (7.4, 8.2 and 9.3) m/s, respectively. This means that the Fe_2O_3 film is most susceptible to shearing and falls off, and the adhesion of NiO is the best. When the film thickness is 10 nm, the critical flow velocities of the three films are (583.3, 782.2 and 1034.2) m/s, respectively, which indicates that the bottom layer of the film is very resistant to physical cutting. At the same time, it is also found that the difference in the critical flow velocity corresponding to several nanoscale films is close to 100 % at most. The closer to the metal surface, the more obvious is the difference in the adhesion of several thin films, and the more obvious is the advantage of NiO as the adhesion of the bottom layer.

Figure 9d shows the relationship between the thickness of various films and the critical flow velocity from 0 m/s to 50 m/s. The figure shows that the thickness of the film corresponding to the critical flow velocity is less than 0.01 mm in a range of 20–50 m/s, and 0.01–0.08 mm in a range of 0–20 m/s. The results show that at high flow velocities, the change in the flow velocity corresponds to a small change in the film thickness, which means that the closer the film is to the substrate, the stronger is the resistance to rupture per unit thickness. However, at low flow velocities below 20 m/s, a small

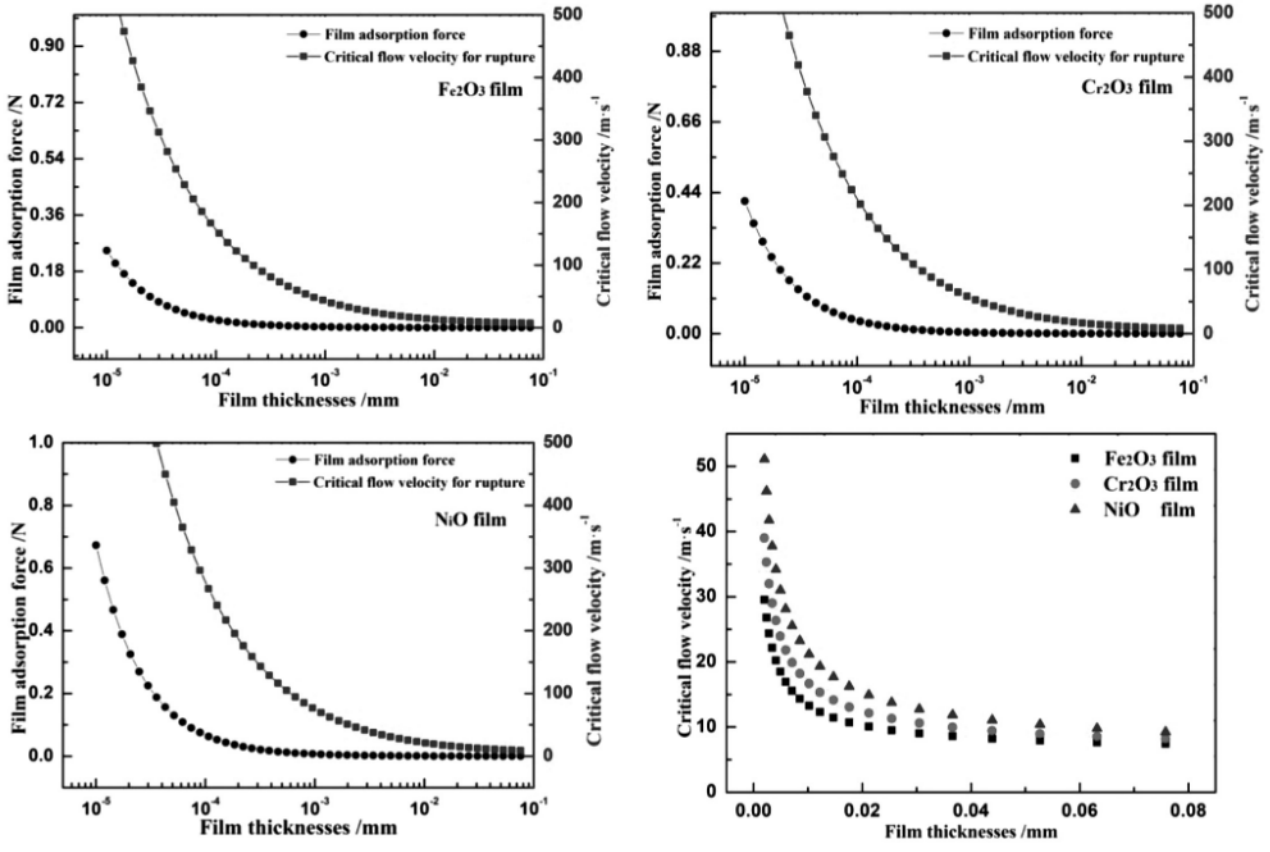

Figure 9: Critical flow velocity of an oxide-film rupture: a) Fe_2O_3 film, b) Cr_2O_3 film, c) NiO film, d) critical flow velocity

range of flow velocities can cause a significant reduction in the film thickness. This shows that the liquid shear force undergoes a process from being simple to complex when peeling the film off the metal surface, and the film with a greater adhesion force is easier to adsorb near the substrate.

5 CONCLUSIONS

In this paper, a high-speed pipe-flow electrochemical-corrosion test was used to test the electric potential, current density and corrosion rate of the 13Cr stainless steel in a flowing Cl-containing liquid. The use of a new small three-electrode system ensured the stability of electrochemical tests in high-speed flowing liquids. The following main conclusions were obtained through experimental measurements and a theoretical analysis:

1) When highly concentrated Cl^- is added to distilled water, the steps of electric potential, current density and corrosion rate appear on the surface of the 13Cr steel. At the same time, the critical flow rate corresponding to the step amount is less affected by the Cl^- concentration.

2) When the flow velocity is lower than the critical flow velocity, the presence of Cl^- has a great effect on the corrosion of 13Cr in the flowing liquid, and when it is greater than the flow velocity, the effect is weakened.

3) The change law for the corrosion rate of 13Cr in distilled water is opposite to that for the Cl-containing liquid. Both the mass-transfer rate for oxygen in the high-speed distilled water and the acceleration of the passivation reaction weaken the corrosion of stainless steel, while the presence of chloride ions changes this trend.

Acknowledgment

The authors appreciate the support of the Scientific Research Program funded by the Shaanxi Provincial Education Department (Program No.20JK0843) and the Foundation of the State Key Laboratory of Petroleum Resources and Prospecting, China University of Petroleum, Beijing (No. PRP/open-2009).

6 REFERENCES

[1] G. A. Zhang, R. F. Cheng, Electrochemical characterization and computational fluid dynamics simulation of flow-accelerated corrosion of X65 steel in a CO_2-saturated oilfield formation water, Corrosion Science, 52 (**2010**) 8, 2716–2724, doi:10.1016/j.corsci.2010.04.029

[2] J. Wang, V. Giridharan, V. Shanov, Z. Xu, B. Collins, L. White, Y. Jang, J. Sankar, N. Huang, Y. Yun, Flow induced corrosion behavior of absorbable magnesium-based stent, Acta Biomaterialia, 10 (**2014**) 12, 5213–5223, doi:10.1016/j.actbio.2014.08.034

[3] U. Lotz, M. Schollmaler, E. Heltz, Flow-dependent corrosion – II. Ferrous materials in pure and particulate chloride solutions, Materials and Corrosion, 36 (**1985**) 4, 63–173, doi:10.1002/maco.19850360405

[4] A. Neville, T. Hodgkiess, J. T. Dallas, A study of the erosion-corrosion behavior of engineering steels for marine pumping applications, Wear, 37 (**1995**) 497–507, doi:10.1016/0043-1648(95)07145-8

[5] S. Nesic, Effects of Multiphase Flow on Internal CO_2 Corrosion of Mild Steel Pipelines, Energy and Fuels, 26 (**2012**) 7, 4098–4111, doi:10.1021/ef3002795

[6] X. Y. Yong, Y. Q. Zhang, D. L. Li, J. Ji , Y. X. Qu, J. D. Wang, Effect of near-wall hydrodynamic parameters on flow induced corrosion, Corrosion Science and Protection Technology, 12 (**2011**) 3, 245–250, doi:10.3354/cr00999

[7] J. J. Liu, Y. Z. Lin, X. L. Tian, X. Y. Yong, X. Y. Li, Numerical simulation of flow induced corrosion of carbon steel in liquid/solid two-phase flow system, Journal of Chemical Industry and Engineering, 55 (**2004**) 2, 232–234, doi:10.1109/JLT.2003.821766

[8] F. Mohammadi, J. Luo, Effects of particle angular velocity and friction force on erosion enhanced corrosion of 304 stainless steel, Corrosion Science, 52 (**2010**) 9, 2994–3001, doi:10.1016/j.corsci.2010.05.012

[9] B. T. Lu, L. C. Mao, J. L. Luo, Hydrodynamic effects on erosion-enhanced corrosion of stainless steel in aqueous slurries, Electrochimica Acta, 56 (**2011**) 1, 85–92, doi:10.1016/j.electacta.2010.09.047

[10] B. T. Lu, J. L. Luo, F. Mohammadi, K. Wang, X. M. Wan, Correlation between repassivation kinetics and corrosion rate over a passive surface in flowing slurry, Electrochimica Acta, 53 (**2008**) 23, 7022–7031, doi:10.1016/j.electacta.2008.02.083

[11] L. R. Goodman, P. M. Singh, Repassivation behavior of X65 pipeline steel in fuel grade ethanol and its implications for the stress corrosion cracking mechanism, Corrosion Science, 65 (**2012**) 12, 238–248, doi:10.1016/j.corsci.2012.08.030

[12] Z. B. Zheng, Y. G. Zheng, X. Zhou, S. Y. He, W. H. Sun, J. Q. Wang, Determination of the critical flow velocities for erosion–corrosion of passive materials under impingement by NaCl solution containing sand, Corrosion Science, 88 (**2014**) 187–196, doi:10.1016/j.corsci.2014.07.043

[13] W. Tian, S. Li, N. Du, S. Chen, Q. Wu, Effects of applied potential on stable pitting of 304 stainless steel, Corrosion Science, 93 (**2015**) 242–255, doi:10.1016/j.corsci.2015.01.034

[14] S. D. Zhu, J. F. Wei, R. Cai, Z. Q. Bai, G. S. Zhou, Corrosion failure analysis of high strength grade super 13Cr-110 tubing string, Engineering Failure Analysis, 18 (**2011**) 8, 2222–2231, doi:10.1016/j.engfailanal.2011.07.017

[15] A. Y. Churyumov, M. G. Khomutov, A. N. Solonin, Comparative study of the stress flow models for high-boron corrosion-resistant steel based on an Arrhenius-type equation and artificial neural networks, Russian Metallurgy (Metally), 2014 (**2014**) 7, 527–531, doi:10.1134/s0036029514070040

[16] S. Jafarzadeh, Z. Chen, F. Bobaru, Computational modeling of pitting corrosion, Corrosion Reviews, 37 (**2019**) 5, 1–21, doi:10.1515/corrrev-2019-0049

[17] U. R. Pedersen, T. B. Schroder, J. C. Dyre, Phase diagram of Kob-Andersen-type binary Lennard-Jones mixtures, Physical Review Letters, 120 (**2018**) 16, 165501.1–165501.5, doi:10.1103/PhysRevLett.120.165501

[18] H. C. Hamaker, The London-van der Waals attraction between spherical particles, Physica, 4 (**1937**) 10, 1058–1072, doi:10.1016/S0031-8914(37)80203-7